ICARUS **135,** 107–126 (1998)
ARTICLE NO. IS985980

Evolution of Lineaments on Europa: Clues from Galileo Multispectral Imaging Observations

P. E. Geissler, R. Greenberg, G. Hoppa, A. McEwen, R. Tufts, and C. Phillips

Lunar and Planetary Laboratory, University of Arizona, Tucson, Arizona 85712
E-mail: geissler@pirl.lpl.arizona.edu

B. Clark, M. Ockert-Bell, P. Helfenstein, J. Burns, and J. Veverka

Laboratory for Planetary Science, Cornell University, Ithaca, New York 14853

R. Sullivan and R. Greeley

Department of Geology, Arizona State University, Box 871404, Tempe, Arizona 85287

R. T. Pappalardo and J. W. Head III

Department of Geological Sciences, Box 1846, Brown University, Providence, Rhode Island 02912

M. J. S. Belton

National Optical Astronomy Observatories, P.O. Box 26732, Tucson, Arizona 85726

and

T. Denk

DLR, Institute for Planetary Exploration, Rudower Chaussee 5, 12489 Berlin, Germany

Received October 7, 1997; revised May 8, 1998

Four distinct classes of lineaments can be described on the basis of Galileo's improved spectral and spatial coverage of Europa: (1) incipient cracks are narrow (<1.6 km wide) and are generally colorless fractures which tend to crosscut other lineament types, (2) ridges have raised relief, tend to be wider (3–6 km) than the cracks, and are distinct in color from the icy plains they transect, (3) triple bands have dim medial stripes similar in color and width to the ridges and broad (8–12 km wide) diffuse low-albedo margins tainted by a red–brown non-ice contaminant, and (4) ancient bands are generally similar in width to ridges and triple bands and have colors intermediate between those of triple bands and the undisturbed icy plains. They are only slightly darker than the plains at visible wavelengths—hence, they were largely undetected by Voyager—but are distinctly brighter than the plains in the infrared, precluding the possibility that they have simply faded from their formerly darker appearance.

The morphologies, spectral properties, and orientations of the lineaments vary systematically with age, suggesting that these four classes represent different stages of development in an evolutionary sequence. Lineament formation appears to be the dominant resurfacing mechanism on Europa, and every landscape that has escaped erasure by heating from below is imprinted with generation after generation of intersecting ridges at various scales and orientations. Relatively recent fractures expose coarse-grained, clean ice in the shallow subsurface, possibly accounting for the distinctive color of the satellite in comparison to the other icy moons of Jupiter. The process of lineament formation may be continuing today; the bright band Agenor Linea is among the leading candidates for current activity.

1. INTRODUCTION

Viewed from a distance, the most striking aspect of Europa is its wreath of global-encircling bands. Voyager images (Smith *et al.* 1979a, 1979b) revealed a criss-crossing network of lineaments on Europa's surface, some extending thousands of kilometers in length. They have also shown evidence for distinct morphological lineament types and indicated age relationships among them (Lucchitta and Soderblom 1982). Among the distinct categories of lineaments mapped by Lucchitta and Soderblom are dark

0019-1035/98 $25.00

TABLE I
Images Used in This Study

Image number	Picture number	Filter	Incidence	Emission	Phase	Latitude range (deg)	Longitude range (deg)	Resolution (km/pixel)
Figs. 2, 3, 4, 13								
349875152	G1E0005	GRN	52.98	22.85	37.39	13.39 89.52	−176.44 −100.67	1.572
349875165	G1E0006	RED	52.65	22.84	37.41	13.31 89.90	−175.60 −99.65	1.572
349875178	G1E0007	VIO	52.77	22.92	37.42	13.39 89.75	−175.76 −99.79	1.572
349875200	G1E0008	756	52.91	22.76	37.43	13.31 89.41	−176.38 −100.65	1.572
349875213	G1E0009	968	52.67	22.79	37.44	13.28 89.76	−175.71 −99.82	1.572
349875226	G1E0010	889	52.72	22.51	37.45	13.08 89.14	−176.34 −100.77	1.572
Fig. 6								
389772500	G7E0040	GRN	47.10	38.29	15.70	27.48 40.47	141.00 152.23	0.5954
389772507	G7E0042	VIO	46.99	38.11	15.75	27.33 40.27	141.04 152.24	0.5950
389773000	G7E0044	968	47.37	37.22	18.66	28.00 39.90	141.37 151.73	0.5748
Fig. 9								
374685439	E4E0028	CLR	74.39	24.90	96.56	5.36 6.17	−34.60 −33.75	0.0257
Fig. 10								
349875113	G1E0002	CLR	61.60	27.39	37.27	−9.98 51.97	−232.22 −140.53	1.572
Fig. 11								
389768800	G7E0030	GRN	36.25	36.27	0.02	25.87 41.86	155.80 172.90	0.391
389768813	G7E0031	VIO	36.12	36.11	0.05	25.74 41.73	155.87 172.93	0.391
389768826	G7E0032	968	35.76	35.73	0.10	25.41 41.32	156.01 172.96	0.391
Fig. 12 C, A, B/D								
383717500	E6E0050	CLR	80.58	38.11	47.99	8.53 10.29	−85.46 −83.09	0.055
383717513	E6E0051	CLR	78.89	36.27	48.53	8.56 10.31	−87.13 −84.86	0.054
383718652	E6E0074	CLR	78.14	46.69	78.62	14.42 15.34	−86.57 −85.91	0.020
Fig. 15								
374649013	E4E0002	CLR	43.75	34.42	55.99	−52.26 −9.08	−142.36 −78.06	1.222
383694600	E6E0001	CLR	40.88	49.02	36.56	−60.64 −26.02	−214.28 −154.83	1.671
383694605	E6E0002	CLR	50.40	41.08	36.20	−60.42 −26.08	−163.16 −133.65	1.668
Fig. 16 A, B, C, D								
VGR2065022	1255J2001	CLR	62.63	31.94	93.70	−61.91 21.31	131.22 226.49	1.776
383694600	E6E0001	CLR	40.88	49.02	36.56	−60.64 −26.02	−214.28 −154.83	1.671
374649013	E4E0002	CLR	43.75	34.42	55.99	−52.26 −9.08	−142.36 −78.06	1.222
360063900	G2E0001	GRN	22.03	23.97	2.17	−88.97 90.0	−157.41 22.59	6.878

bands, triple bands (dark bands having a bright, central stripe), gray bands (intermediate in albedo between the dark bands and the background icy plains), small raised ridges and arcuate ridges, and short, stubby wedge-shaped bands concentrated near the equator. The oldest of these are generally gray bands, such as those located at high southern latitudes on the leading side of Europa, while the youngest lineaments, as determined by superposition and crosscutting relations, are the ridges. The europan lineaments have been generally interpreted as extensional in origin and variously attributed to tidal flexing (Helfenstein and Parmentier 1980), long-term orbital evolution (Helfenstein and Parmentier 1983), and nonsynchronous planetary rotation (Helfenstein and Parmentier 1985, McEwen 1986a).

Galileo data have expanded our knowledge of europan lineaments in two important ways. First, high-resolution images down to 6 m/pixel have sampled the lineaments at various locations, frequently at high solar incidence angles near the terminator. For comparison, the best Voyager images were 2 km/pixel. Second, while multispectral images recorded by Voyager were limited to wavelengths less than 0.59 μm, Galileo's Solid State Imaging (SSI) system is sensitive to wavelengths up to 1 μm, extending the spectral range of the images into the near-infrared. Detailed descriptions of the imaging system are given by Belton *et al.* (1992) and Klaasen *et al.* (1997); filters used to date for Europa color imaging are designated "violet" (413 nm effective wavelength when illuminated by white light; Klaasen *et al.* 1997), "green" (560 nm), "red" (665 nm), "756" (757 nm), "889" (888 nm), and "968" (991 nm). Four sets of color observations have so far been obtained of Europa from Galileo, at resolutions ranging from 390 m/pixel to 6.9 km/pixel (Table I). Targets for color imaging included the Tyre impact structure at 34° N, 146.5° W at 589 m/pixel resolution during Galileo's seventh orbit (G7)

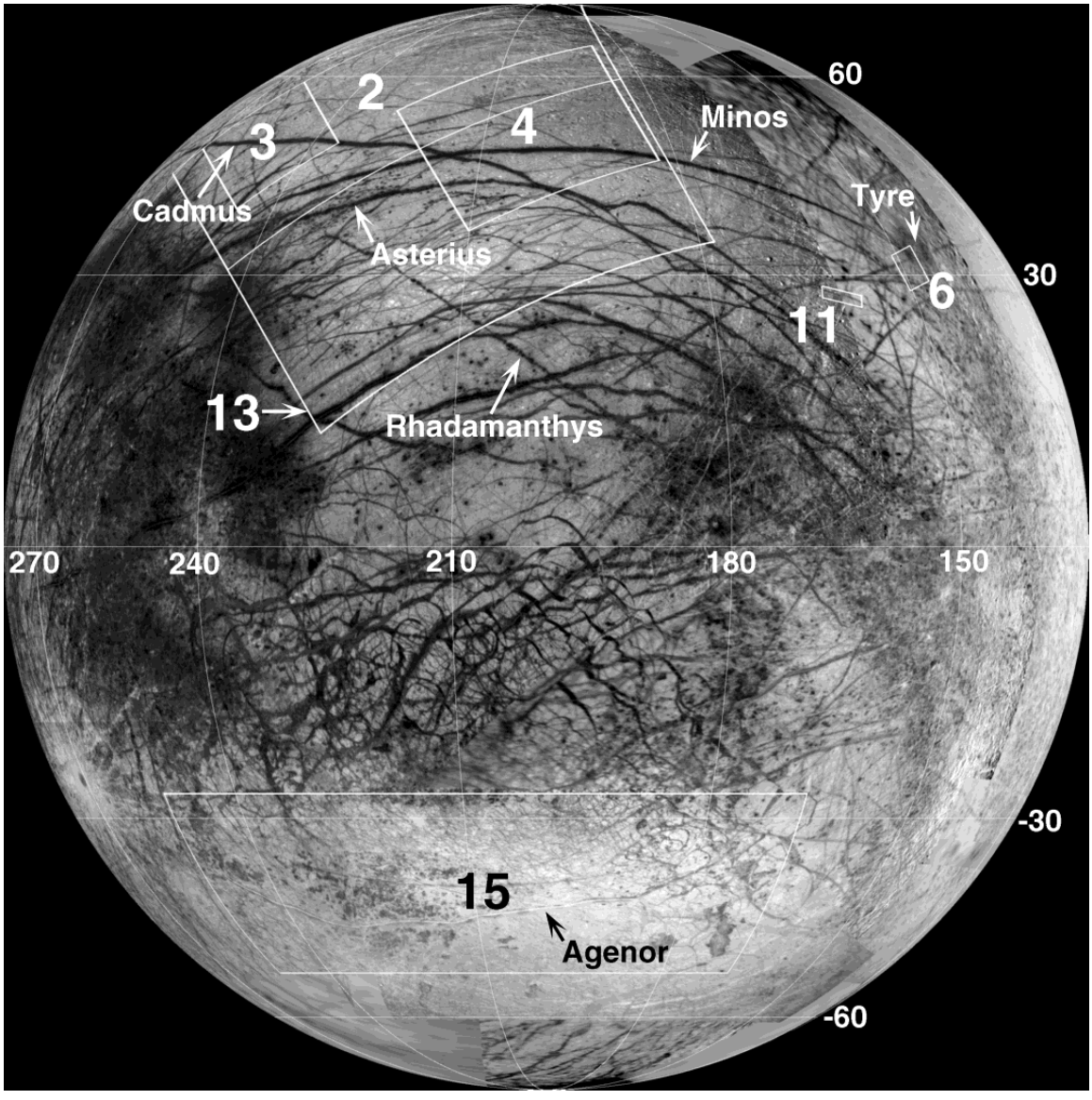

FIG. 1. Location diagram (mosaic of data from Voyager and Galileo orbits G1 to G7). Orthographic projection of the trailing hemisphere centered at 0°N, 200°W. Outlines show positions of numbered figures.

(Moore *et al*. 1998), an image of the spacecraft's shadow point at 30° N, 162° W at 390 m/pixel also during G7 (Helfenstein *et al*. 1998), and a global view of the trailing hemisphere centered at 1° N, 293° W acquired at 6.9 km/pixel during encounter G2. The most comprehensive coverage was obtained of Europa's northern high-latitude region at 1.6 km/pixel resolution and 37° phase angle from a nontargeted flyby during Galileo's first (G1) orbit of Jupiter (Belton *et al*. 1996). The imaged region extends across the trailing side of the antijovian hemisphere of Europa (longitudes 180 to 270), centered at 45° N, 221° W (Fig. 1). Four-color coverage extends across the entire region, obtained with the violet, green, 756, and 968 filters, and data from two additional filters (red and 889) were partially returned.

The importance of the new spectral coverage can be seen from Fig. 2, which compares visible and near-infrared images of the region for which all six-color data are available. The top panel (Fig. 2A, a red–green–violet composite) approximates the visual appearance of Europa, except that a violet filter image is used to portray blue. No photometric correction has been applied; illumination is from the southwest (lower left) and the surface darkens as the terminator is approached, toward the right. At visible wavelengths, and to Voyager's camera, the lineaments appear in shades of brown with a maximum contrast of ~50%

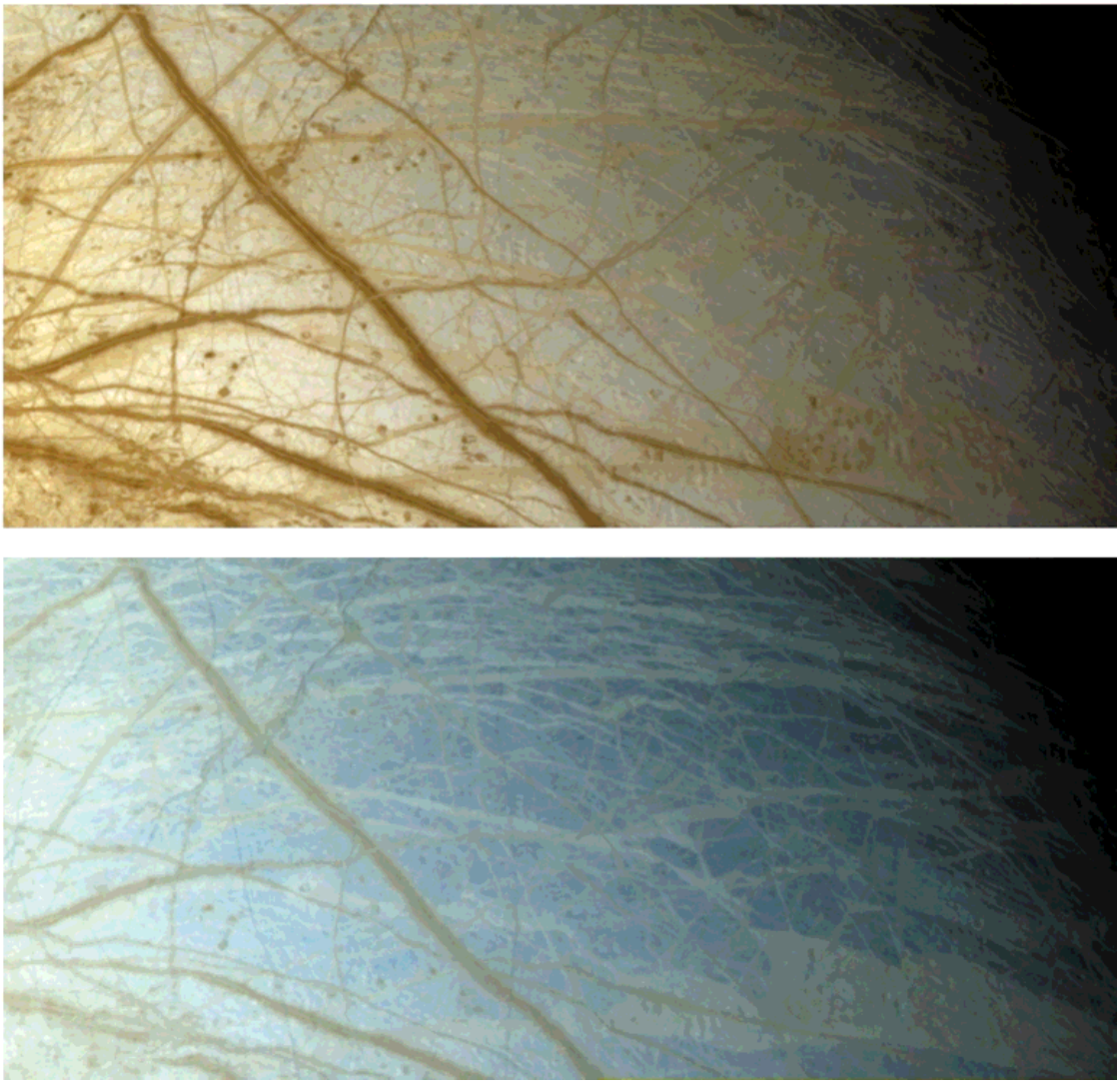

FIG. 2. Comparison of visible and near-infrared images of europan lineaments: (top) red, green, violet composite, (bottom) false color composite with 968-, 889-, 756-nm filter images shown as red, green, and blue (picture numbers G1E0005–G1E0010).

(in the violet filter). In the near-infrared, however, these lineaments display a diversity of colors unseen by Voyager (Fig. 2B, a false-color composite in which the 968, 889, and 756 filter images are shown as red, green, and blue, respectively) and allow us to map bands barely distinguishable at shorter wavelengths.

In this paper, we discuss Galileo's new insights into the formation and evolution of Europa's lineaments, concentrating on the color observations but drawing analogies to features seen at higher resolution elsewhere on Europa (no very high resolution data have yet been acquired in the areas with color coverage). We will show that europan lineaments exhibit systematic changes in morphology, spectral properties, and orientation with age, and we suggest a possible sequence of development and offer interpretations for the evolution of these intriguing features.

2. CLASSIFICATION OF LINEAMENTS

2.1. Morphology and Superposition Relationships

Figure 3 is a close-up of a region of intersecting lineaments, about 350 km across and centered at 48° N, 250° W. Linear features of different ages can be seen to have a variety of morphologies and associated color characteristics in this 968, 756, and violet filter composite (shown here as red, green, and blue). The youngest of these is a dark, 1-pixel-wide line running from top to bottom of the picture (labeled F1 in Fig. 3). This fracture is no wider than the dimensions of a pixel (1.6 km) and crosscuts, i.e., is younger than, every other lineament in the scene. It is darker than but similar in color to its surroundings and exhibits no discernible relief along its thousand kilometer length, only

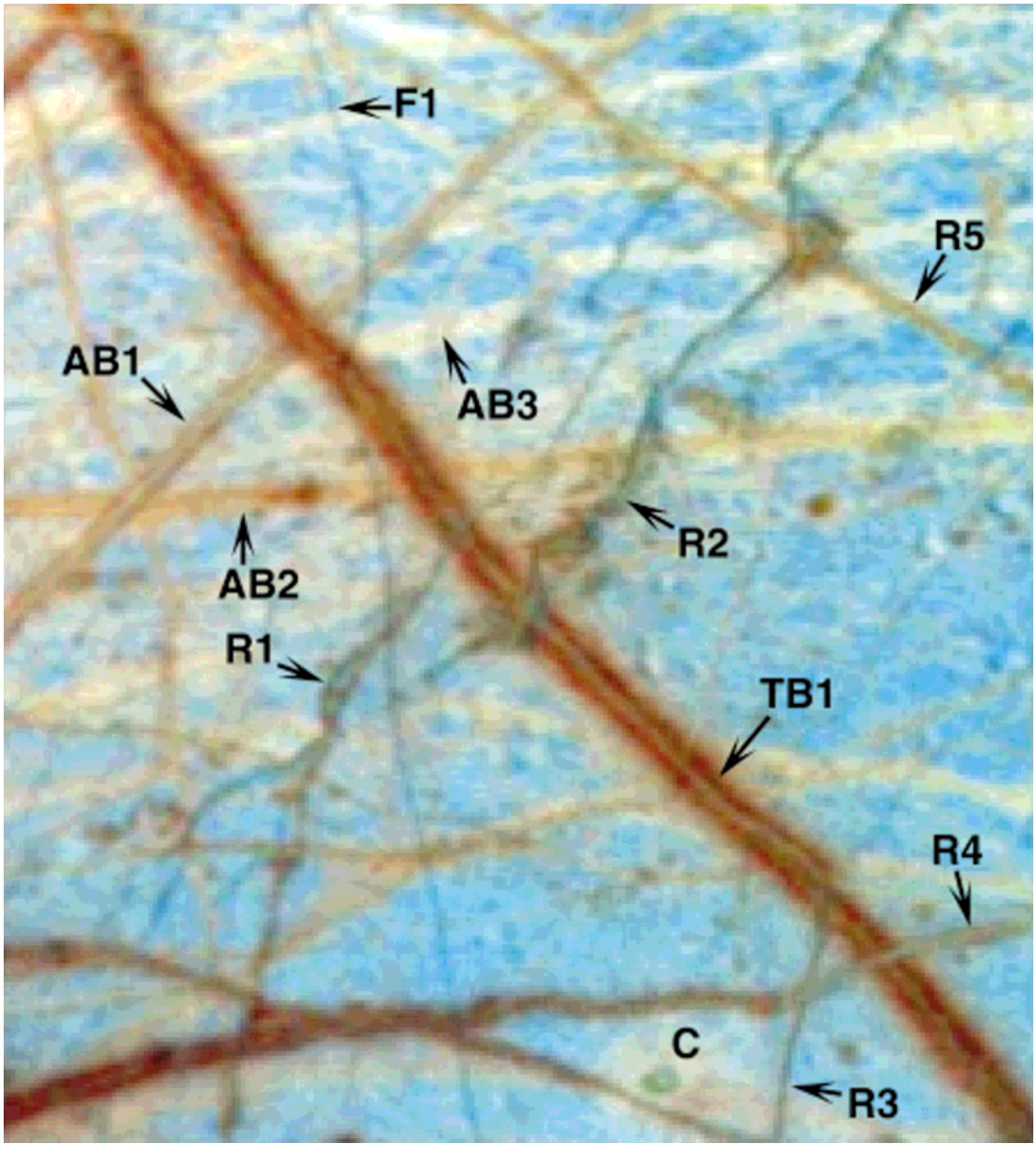

FIG. 3. Close-up of a region of intersecting lineaments about 350 km across and centered at 48°N, 250°W. Composite of 968, 756, and violet images. Labeled are simple fractures (F), ridges (R), triple bands (TB), and ancient bands (AB). The prominent triple band TB1 is Cadmus Linea (picture numbers G1E0005–G1E0010).

a portion of which is shown here. It curves as it crosses Cadmus Linea (TB1 in Fig. 3), suggesting that it is a tension crack rather than a transform fault. This feature is representative of a class of lineaments formed by the most recent (perhaps current) stresses at their locations. By analogy to features seen at much higher resolution elsewhere on Europa, these ''incipient cracks'' will later be identified with simple fractures lacking associated marginal ridges, or having at most a single pair of ridges below the resolution limit (Section 4).

Slightly wider bands, 2 or more pixels across, are distinct in color from the icy plains and can be seen to have raised relief when viewed near the terminator. Several examples appear in slightly greenish hues in Fig. 3 (bands R1 to R5), indicating a reduced 968-nm filter reflectance. The color characteristics of these ridges are shared by the dim medial stripes at the cores of triple bands like Cadmus (TB1), contrasting with the diffuse red–brown materials at their margins. Subtle color differences can be seen, for example, at the intersection of an irregular ridge (R2) with Cadmus

Linea near the center of the picture. Greenish hues indicating reduced 968-nm reflectance are also seen in the dark central portion of the crater at the bottom of Fig. 3.

Next in age after the ridges is Cadmus Linea (TB1), an example of a fully developed triple band. The brown coloration extends in both directions 8 to 12 km from the center of the band, varying remarkably little along the great length of this lineament. Cadmus crosscuts many older lineaments (representatives are labeled AB1, AB2, and AB3 in Fig. 3), which appear white or in pale orange and yellow shades in the false color composite. On the whole, these ''ancient bands'' are indistinct in visible light (Fig. 2A) but notably brighter than the surrounding icy plains at infrared wavelengths. At least one (band AB1) retains a bright medial stripe, similar to the darker triple bands.

These four classes of lineaments—cracks, ridges, triple bands, and ancient bands—are seen again in Fig. 4, an enlargement of the eastern portion of the six-color data set shown as a 968, 756 and violet filter false-composite which has been photometrically corrected to compensate for near-terminator darkening (details of the correction are given in Section 5). This scene is about 575 km in width and is centered at 50° N, 202° W. Lineament F2 (labeled in Fig. 4) appears to be a simple fracture less than a pixel in width, devoid of relief, and invisible in color ratio images. Band R5, also shown in the previous figure, can be clearly seen to be a ridge: its western (sun-facing) slope is bright in comparison to the opposite side. Seen at high resolution, ridges on Europa commonly occur in symmetric pairs or as multiple-ridge sets with central valleys (Greeley *et al.* 1998), but the detailed topography of R5 cannot be made out at this resolution. Its green color, again indicating reduced 968-nm reflectance, contrasts markedly with both the blue background plains and the reddish brown of triple bands TB2 and TB3, which it crosscuts.

Dark brown units in this region include isolated spots as well as the prominent triple bands Cadmus (TB1), Minos (TB3), and Asterius (TB4) Lineae. Asterius has a crenulated margin, unlike the more regular curvilinear shapes typical of triple bands. Several indistinct, brighter bands crossing from left to right near the center of Fig. 4 (such as AB4) represent the oldest lineaments preserved in the region. These wispy traces are actually brighter than the surrounding plains at infrared wavelengths, and they can be traced for hundreds of kilometers. Their widths are on the order of 4.5 to 6 km, similar to that of the ridges. The bright wedge near the top of the picture (AB5) appears similar in age to the ancient bands on the basis of superposition relationships. Like the ancient bands, it is brighter than adjacent, undisturbed plains in the near-infrared but slightly darker at visible wavelengths (see Section 2.2). In this respect, the bright wedge AB5 is similar to the gray bands identified in the southern hemisphere by Lucchita and Soderblom (1982) from Voyager images. Pappalardo and Sullivan (1996) interpret the southern hemisphere gray band Thynia Linea to have formed by crustal extension. The bright wedge in Fig. 4 is much wider than other linear features in the region and could be an ancient pull-apart zone which has brightened with age.

The relative ages of these various lineament types are well shown by the four-way intersection near the top of Fig. 4: the narrow incipient crack F2 crosscuts ridge R5, which in turn postdates triple band TB2. All of these events overprinted the bright wedge AB5, the oldest in the sequence. The orientation of these particular lineaments appears to rotate systematically in a clockwise sense with decreasing age, a point we shall return to in Section 5.

2.2. Color and Albedo Properties

The spectral properties of the lineaments vary markedly with illumination and viewing geometry and with geographic location on Europa. Lineaments and mottled terrain on the trailing hemisphere are much redder than their yellowish counterparts on the leading side, probably due to the exogenic effects of charged particles (McEwen 1986b). We can minimize differences due to photometric and exogenic effects by comparing the colors of representative features from nearby locations in the area of G1 color coverage. The spectral variability of these features is examined by Clark *et al.* (1998), who also estimate absolute normal albedos for the units.

As previously mentioned, the *incipient cracks* are notable for their lack of distinguishing color—these thin ''pencil lines'' darken both bright and dark terrains equally, independent of wavelength. This is illustrated in Fig. 5, which compares the six-filter SSI spectra of various lineaments with the color of the surrounding plains, measured from nearby locations to minimize differences in illumination and viewing geometry. These data are plotted in units of radiance factor R_F, the ratio of the observed radiance to that expected from a normally illuminated Lambertian target at the same heliocentric distance, and were extracted from images calibrated with procedures derived by Klaasen *et al.* (1997). Figure 5 shows that fracture F1 is darker than, but similar to the neighboring icy plains in color. The spectrum is contaminated by the plains, since the fracture is less than a pixel wide, but comparing the two spectra suggests that topographic shadows along the fracture may simply darken the plains, leaving the color unchanged.

Even though the fractures have no intrinsic coloration, they may expose subsurface materials which are distinct in color from the surficial deposits. This is especially apparent in the region near the Tyre impact structure (Fig. 6). Relatively young fractures imaged at 589 m/pixel in this area are actually brighter than the average icy plains material in the violet and green filters (by about 15 and 7%,

respectively) and have much deeper absorptions in the 968-nm filter. These features were presumed to be ridges until recently, when higher resolution (170 m/pixel) near-terminator images obtained in orbit E14 showed them to be simple cracks a few hundred meters across. The high albedo of the fractures can be explained if they expose relatively clean ice, whereas the 1-μm absorption is attributed to relatively large grain sizes in comparison to the surface materials. The long wavelength filters of SSI are sensitive to ice grain size, particularly since the camera's 968 filter lies on the shoulder of the weak water ice absorption band at 1.04 μm. For example, Galileo multispectral imaging observations of Antarctica taken as the spacecraft flew past Earth en route to Jupiter (Geissler *et al.* 1995) yield 968/green ratios near unity for continental snows (average grain diameters of a few tens of micrometers) decreasing to ~0.85 for shelf and sea ice (diameters of several hundred micrometers). The 968/green ratio for the young fractures in Fig. 6 averages ~0.93 +/− 0.02. This comparison suggests that the mean ice grain diameter of shallow subsurface ice in the Tyre region is on the order of 100 μm or larger. The deep 1-μm absorption of the near-surface ice may explain Europa's relatively "blue" color in comparison to the other icy Galilean satellites; Ganymede and Callisto have much redder near-infrared spectral slopes than Europa, even allowing for spectral mixing with the dark contaminants on their surfaces (Geissler *et al.* 1996).

Ridges display a great variety of colors and albedos, possibly related to their age. Figure 5 shows that the "green" ridges in the 1.6-km/pixel G1 data are spectrally distinct from both the background icy plains and the dark triple band margins. Ridge R2 (Fig. 3) is similar in color to the dark margins of Cadmus Linea, but is brighter and has a deeper 1-μm absorption. The bright core of Cadmus has similar but less pronounced color characteristics. Color observations at higher resolution during G7 (Fig. 6) confirm that these spectral properties are common to ridges. Ridge doublet R6 is bright and blue in comparison to its surrounds, similar to the ridges at the cores of triple bands TB5 and TB6, suggesting that the ice was relatively clean at the time it was extruded.

The distinguishing characteristic of *triple bands* is not the dim medial cores, which resemble less adorned ridge sets elsewhere on Europa, but the dark, diffuse coloration extending 8–12 km from the central ridges. At high resolution, triple bands can be seen to be composed of sets of up to 8 parallel ridges, with darkened and somewhat subdued topography along their margins. The discoloration seems to be confined to the surface: fracture F3 in Fig. 6 appears to cut across the dark margins of triple bands TB5 and TB6, revealing clean, coarse-grained ice just below the surface. The spectrum of Cadmus' dark margins (TB1 in Fig. 5) represents our best estimate to date of the visible and near-infrared reflectance of the darker, nonice contaminant on Europa's trailing hemisphere. This material is strongly absorbing in the violet (and ultraviolet, from Voyager observations, Johnson *et al.* 1983, McEwen, 1986b) and exhibits a steep positive spectral slope (red color) up to 1 μm. These characteristics are remarkably consistent between exposures of the red–brown contaminant across the trailing hemisphere as seen in the G2 global color imaging observations, including thermally disrupted ("ice-raft") terrain and the continuous ejecta from recent impact craters like Pwyll. Slight differences can probably be assigned to variations in the water abundance and grain size of ice/contaminant mixtures (see also Clark *et al.* 1998). The identity of the contaminant remains elusive at this writing; Galileo Ultraviolet Spectrometer (UVS) observations associate exposures of the red–brown materials with deep absorptions at 0.28 μm, attributed to sulfur compounds such as SO_X (Hendrix *et al.* 1996), while Galileo Near Infrared Mapping Spectrometer (NIMS) results suggest heavily hydrated materials such as hexahydrite ($MgSO_4 \cdot 6H_2O$) (Fanale *et al.* 1998, McCord *et al.* 1998). Such salts and sulfates are colorless at visible wavelengths, however, requiring an additional compositional component to account for the coloration.

Europa's *ancient bands* were noted to brighten with age on the basis of Voyager observations, and it was assumed that these features progressively reverted over time to the color and albedo of the undisturbed icy plains (e.g., Pappalardo and Sullivan 1996). However, the bands do not merely fade away, but rather brighten beyond the plains' albedo, especially at long wavelengths. Figure 7 demonstrates the phenomenon by comparing lineaments of three different ages. Cadmus Linea (spectrum TB1) is the youngest of the three, overprinting an older lineament (AB1) which still retains a recognizable triple band albedo pattern. Both crosscut an ancient band (AB3) which is darker than the background plains at short wavelengths but considerably brighter in the near-infrared. This spectral behavior, common among the oldest lineaments imaged, produces a contrast reversal with wavelength; ancient bands are slightly darker than ice at visible wavelengths, but unexpectedly bright at infrared wavelengths not seen by Voyager. Unfortunately, the crossover point is near the middle of SSI's spectral range, making the older lineaments indistinct in the clear filter used for most Europa imaging in the nominal mission (Fig. 1). Ancient bands and wedges are intermediate in color between the icy plains and the dark red–brown component and appear to be mixtures of these two end members (Fig. 8). This conclusion is supported by the linear spectral mixing models of Clark *et al.* (1998), who extend the analysis to include the isolated spots ("lenticulae") which make up Europa's mottled terrain; most of the endogenic spectral variability on Europa's trailing hemisphere can be adequately accounted for by

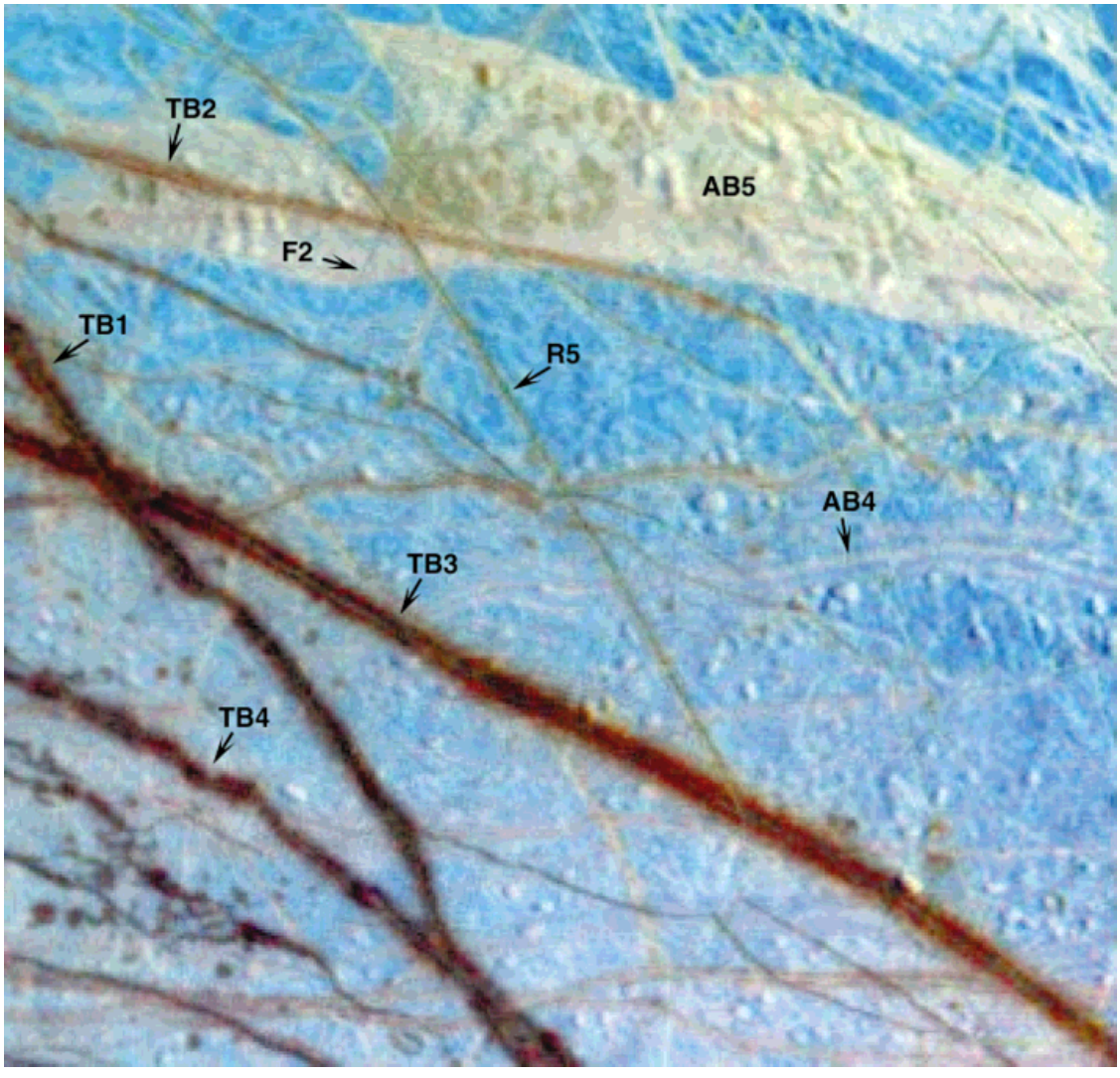

FIG. 4. Close-up of a region of intersecting lineaments about 575 km across and centered at 50°N, 202°W. Composite of 968, 756, and violet filter images. Labeled are simple fractures (F), ridges (R), triple bands (TB), and ancient bands (AB). Shown is the intersection of Cadmus (TB1) and Minos (TB3), with Asterius Linea (TB4) to the south (picture numbers G1E0005–G1E0010).

mixtures of the dark brown contaminant with ice of various grain sizes. The fact that the color of the ancient bands is intermediate between those of the dark contaminant and ice units, but their long-wavelength albedos exceed that of either end-member, implies that the brightening is intrinsic to the ancient bands. It cannot be due to simply blanketing both the bands and the plains with a mantling deposit, for example. Instead, a local frost deposit or reduction in the grain size of the icy matrix or the dark contaminant is required (or the production of a spectrally neutral brightening agent from the breakdown of the red–brown material).

In summary, four distinct classes of lineaments can be described on the basis of Galileo's improved spectral and spatial coverage of Europa: (1) incipient cracks are narrow ($<$1.6 km wide) and are generally colorless fractures which tend to crosscut other lineament types, (2) ridges have raised relief, tend to be wider (3–6 km) than the cracks, and are distinct in color from the icy plains they transect, (3) triple bands have medial stripes similar in color and width to the ridges, and broad ($\sim$10 km wide) diffuse low-albedo margins tainted by a red–brown nonice contaminant, and (4) ancient bands are generally similar in width to ridges and triple bands and have colors intermediate between those of triple bands and the undisturbed icy plains. They are only slightly darker than the plains at visible wavelengths—hence, they were largely undetected by Voyager—but are distinctly brighter than the plains in the infrared, precluding the possibility that they have simply faded from their formerly darker appearance. In the

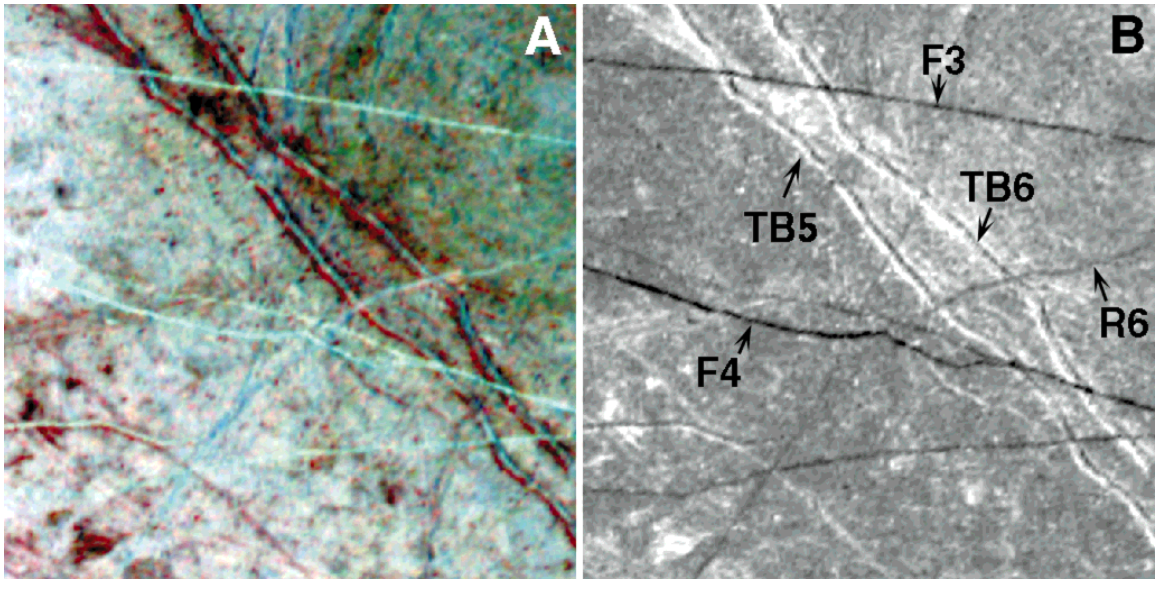

FIG. 6. Fractures, ridges, and triple bands in the Tyre region. Image is about 115 km across and centered on 32°N, 148°W. (A) The youngest lineae are both brighter and bluer than the average icy plains in this false color (968, green, and violet filters) composite. (B) 968/green color ratio image scaled so that a ratio of 1.3 appears white, 0.9 black. Labeled are simple fractures (F), ridges (R), and triple bands (TB). Relatively recent fractures expose coarse-grained ice, which appears dark due to absorption in the 968-nm filter (picture numbers G7E0040, G7E0042, and G7E0044).

next sections we will show examples of lineaments transitional between these four classes and suggest an evolutionary sequence which implies that these diverse features represent the results of a single set of processes seen at different stages of development.

3. TRANSITIONAL LINEAMENTS

Important clues to the sequence of development of cracks, ridges, and bands are found among examples of features transitional from one lineament type to the next. Europan lineaments range up to thousands of kilometers in length and tend on the whole to be remarkably uniform over great distances. Longitudinal variations may be caused by changes in strain history with location or by local or regional differences in the properties of the lithosphere, such as thickening of an ice shell toward the pole (Ojakangas and Stevenson 1989a).

Examples of cracks which grade into double-ridges are surprisingly rare in the high-resolution Galileo images returned to date, despite the preponderance of both lineament types. One lineament suggestive of this transition intersects Asterius Linea at 13.7° N, 272° W, just north of the intersection of triple bands Asterius and Agave. This crack shows little evidence of positive relief at the point it crosses Asterius, but grades southward into a prominent if modestly sized double ridge over a distance of less than 30 km. Other possible examples originate in the large ringed impact structures Tyre (Fig. 6, ridge R6) and Callanish, at 16.5° S, 333° W, where they are expressed as

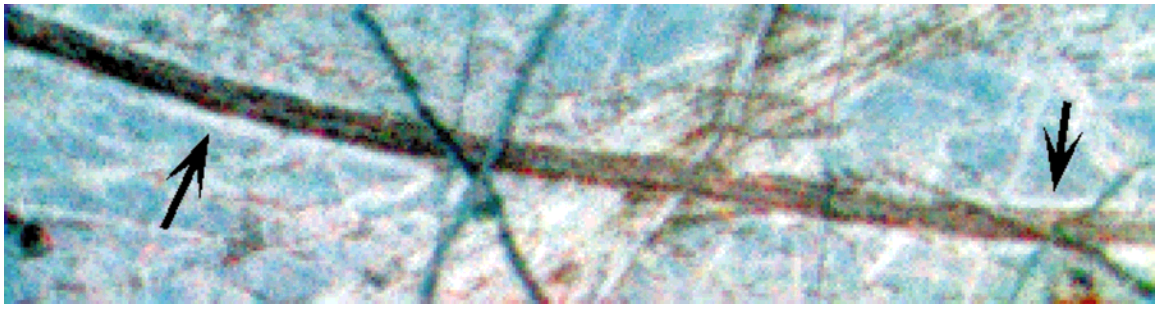

FIG. 11. Feature transitional between triple bands and ancient bands located at 28°N, 161°W. Arrows point out bright margins of dark material flanking the central ridge (picture numbers G7E0030–G7E0032).

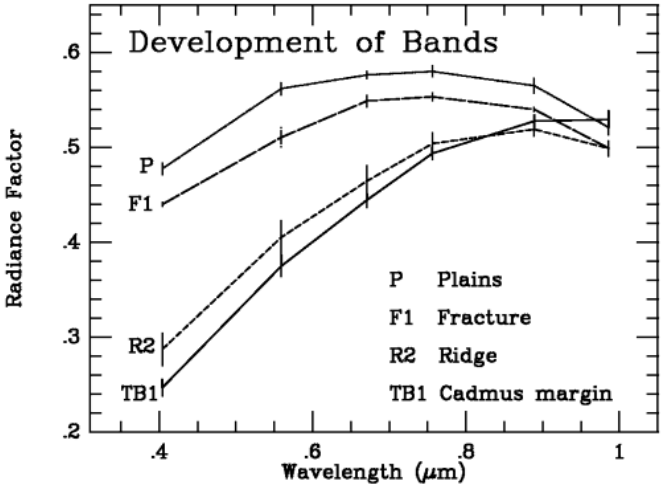

FIG. 5. Six-filter SSI spectra comparing colors of developing lineaments with the surrounding ice plains. Labels refer to features shown in Fig. 3. Error bars represent the standard deviation within each sampled location.

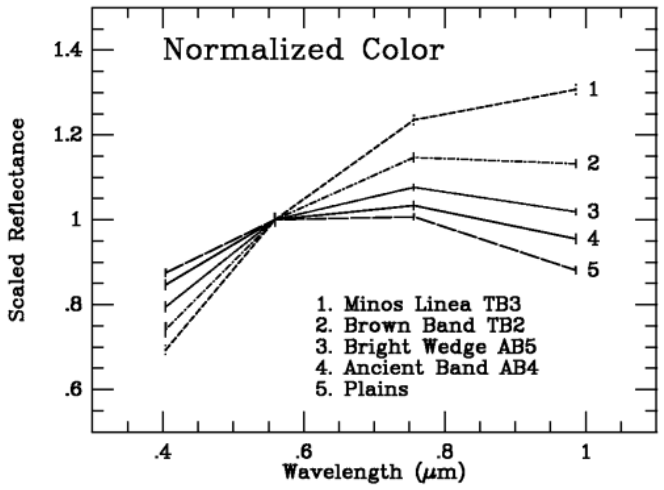

FIG. 8. SSI spectra of various lineaments normalized to unity green-filter reflectance. Ancient bands and wedges are intermediate in color between the icy plains and the dark red–brown triple band margins and appear to be mixtures of the two end members. Labels refer to features shown in Fig. 4. Error bars represent the standard deviation within each sampled location.

fractures showing little positive relief within the macula, but grow in stature as they radiate outward into less disrupted (and presumably more competent) terrain. A small-scale structure connecting two nearby regions of disrupted terrain at 11° N, 327.5° W displays unusual morphological variations along its length (Fig. 9). Both ends of this 15-km long crack terminate in disrupted terrain, the westernmost of which is vaguely circular and possibly of impact origin. The rough surface and irregular planform of the crack's marginal ridges give this feature a freshly formed appearance, in contrast to the more regular shapes of typical double ridges. The eastward bifurcation of the crack is also very uncommon; most lineament intersections occur where one lineament clearly overprints another.

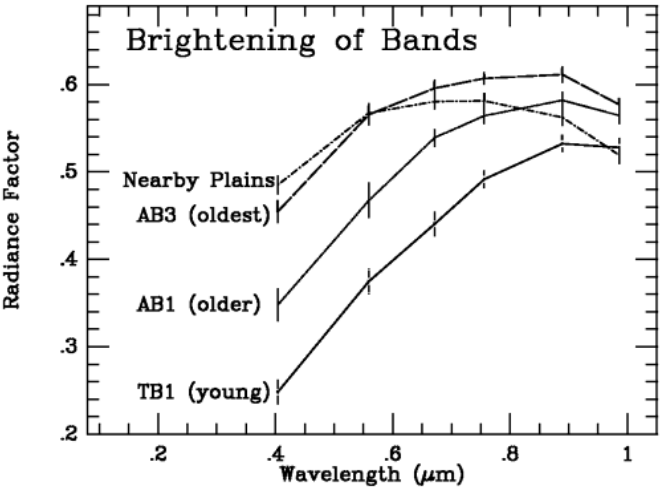

FIG. 7. SSI spectra of lineaments of three different ages. Europa's ancient bands brighten beyond the albedo of the background plains, particularly at long wavelengths. Labels refer to features shown in Fig. 3. Error bars represent the standard deviation within each sampled location.

Examples of features transitional between ridges and triple bands are comparatively common. Several are seen in Fig. 3. At the bottom of the picture, ridge R4 grades to the southwest (left) into a fully developed triple band complete with gradually widening red–brown staining. Another gradual transition can be seen by following ridge R5 eastward; its orange–brown color in Fig. 3 changes slowly along its length to a more greenish appearance in Fig. 4, an effect perhaps contributed to by the changing illumination and viewing geometry (Fig. 4 is nearer the terminator). In contrast to these gradual transitions, many lineae darken at discrete points along their lengths. Irregular discoloration is associated with ridges R1 and R2 in Fig. 3, notably at their intersections with other lineae.

Rhadamanthys Linea (Fig. 10) is remarkable in that it may represent a ridge ''caught in the act'' of forming a triple band (Belton *et al.* 1996). Dark brown spots have formed along its length that are indistinguishable in color from more fully developed triple bands such as Minos and Cadmus. Other bands appear transitional in morphology between Rhadamanthys and the more common triple bands that are uniform along their lengths. We have already remarked on the crenulated margins of Asterius Linea (Figs. 1 and 4, TB4), which appears as though a multitude of spots coalesced along its length. Two examples of double ridges with discontinuous dark discoloration

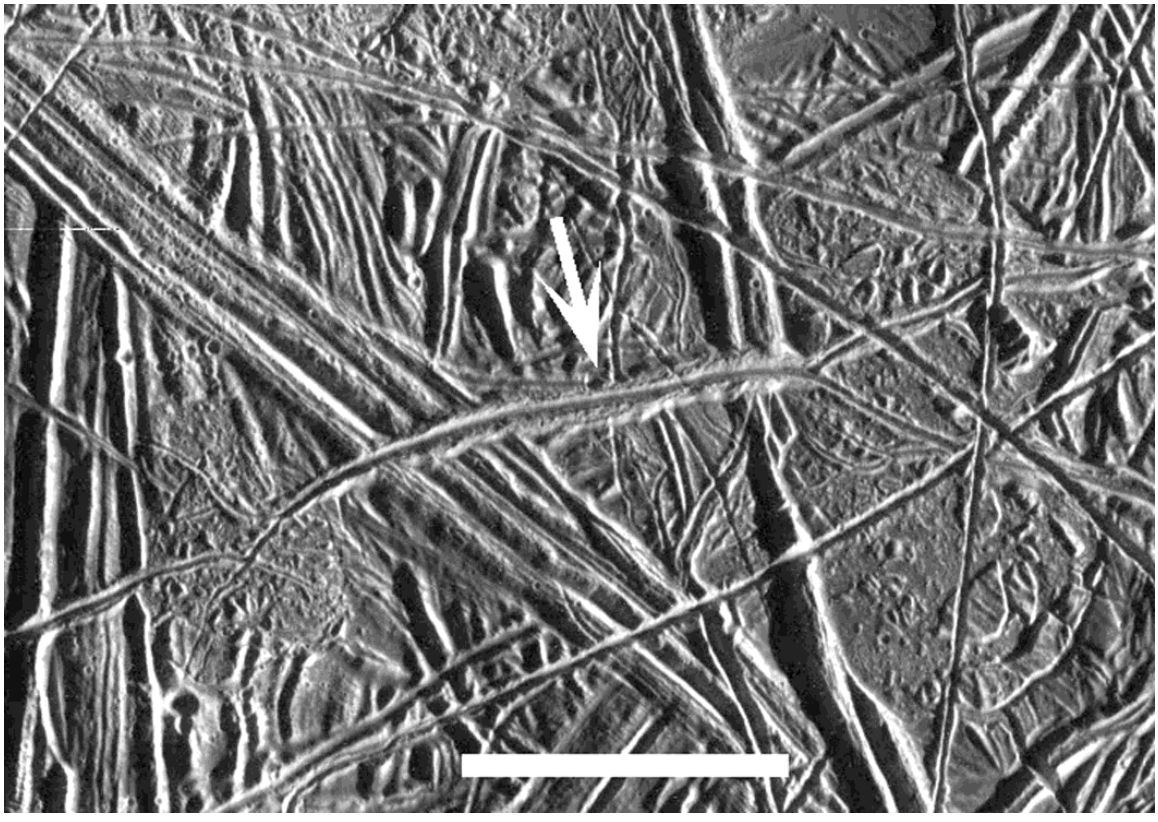

FIG. 9. Feature transitional between fractures and double ridges, located at 11°N, 327.5°W. Scale bar is 5 km long (picture number E4E0028).

along their flanks were imaged at 420 m/pixel during Galileo's third (C3) orbit at 13.5° S, 196° W in a region of dark, wedge-shaped extensional tectonic features west of the antijove point (Greeley *et al.* 1998). These particular ridges have a knotty appearance, and the larger relief sections of the ridges occupy the centers of the localized dark spots. The implication is that activity along the fracture, i.e., ridge building, is related to the degree of darkening of adjacent ice surfaces.

Bands in the process of brightening make up the final group of transitional lineaments. As already noted, band AB1 in Fig. 3 is intermediate in color and albedo between Cadmus Linea (TB1) and the ancient bands crosscut by both lineaments (see Fig. 7), yet still retains the distinctive albedo pattern of a triple band. Other triple bands can be seen to have brightened at their outermost margins. A bright margin is faintly visible on Minos Linea (TB3) in Fig. 4, but is better detailed by spectral mapping of the lineae as discussed in Section 5. A better example was photographed in a color imaging sequence on Galileo's 7th orbit (G7) at 28° N, 161° W (Fig. 11). This small (5 km wide) triple band has margins which are brighter in all three filters (violet, green, and 968 nm) than its interior, as well as an indistinct dim medial core. This example indicates that the bands do not brighten uniformly across their surfaces, but brighten from the outside inward instead. The brightening of europan terrain is not restricted to the lineaments; it is also apparent among the dark wedges interrupting older plates in the equatorial region (Greeley *et al.* 1998, Fig. 18).

4. SEQUENCE OF DEVELOPMENT

Based on the observations described above, we suggest that the various europan lineaments do not develop by separate processes, but instead they are genetically related and evolve through the sequence of morphological stages outlined in Table II. Analogous landforms selected from high-resolution imagery obtained elsewhere on Europa are shown in Fig. 12 to illustrate these stages. Initially, lineaments form as simple fractures of the brittle crust with little perceptible positive relief (Fig. 12A). Marginal ridges are built up over time on the flanks of favorably oriented fractures (Fig. 12B). The paucity of features transitional from cracks to double ridges may reflect the rapidity of the ridge-building process once begun. Ridges may increase in size until their weight exceeds the limiting load that can be supported by the crust, which bends and buckles under

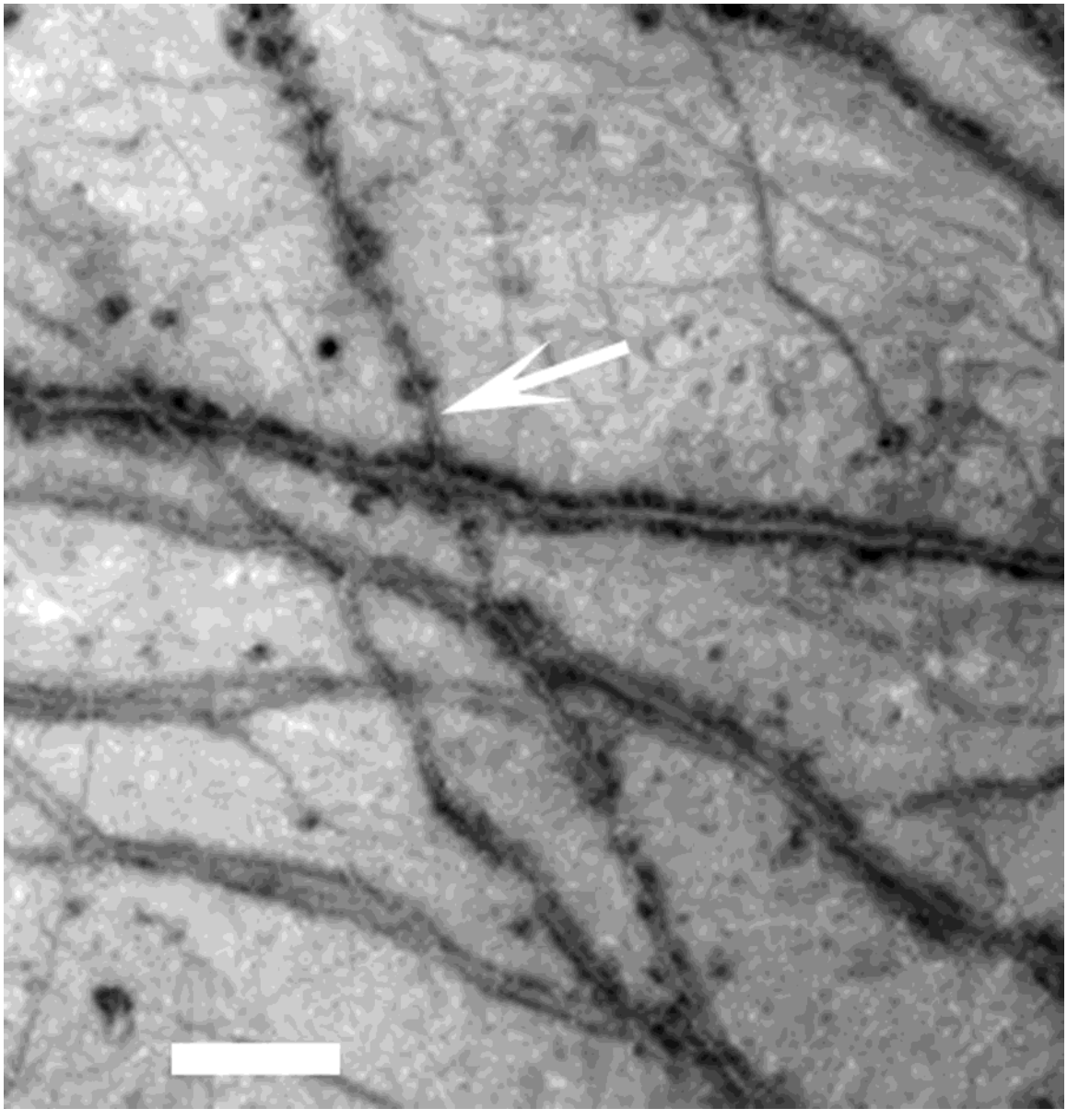

FIG. 10. Rhadamanthys Linea, a feature transitional between ridges and triple bands. Image centered at 18.5°N, 198°W. Scale bar is 50 km (picture number G1E0002).

the stress (cf. Pappalardo and Coon 1996); note the small fractures parallel to the ridge set in Fig. 12B. In some cases, repeated activity along the lineaments apparently takes advantage of these parallel fractures, and the ridges enlarge to form multiridged structures such as those found at the center of the largest triple bands (Fig. 12C) (c.f. Greenberg *et al*. 1998). Triple bands apparently form only after activity along the largest lineaments ceases; all the triple bands so far imaged at high resolution are crosscut by younger features and inferred to be presently inactive (small cracks can be seen to crosscut the triple band in Fig. 12C, for example). The ridges at the core of triple bands retain their appearance to some extent while icy surfaces immediately adjacent to the ridges darken and local preexisting topography is erased, possibly as the ridges sink under their own weight. Finally, the ridges relax and reequilibrate (Fig. 12D), and the bands brighten beginning with their outermost margins.

The net effect of these processes is to create a surface everywhere overprinted with a dense network of superposed ridges. Regions referred to here as ''plains'' can in fact be seen at high resolution to be made up of complex

meshes of ridge sets. Ridge-building is the dominant process shaping the moon's surface, and every landscape that has escaped erasure by heating from below is imprinted with generation after generation of intersecting ridges at various scales and orientations. Relief along these older ridge sets is subdued in comparison to younger terrains, suggesting that the ridges viscously relax over time.

Specific conditions must be met at each step of this sequence, and not all lineaments necessarily evolve from one stage to the next. Fractures must remain active for extended periods before marginal ridges can be built up. The brown margins along triple bands may be visible only after activity ceases and the ridges sink, a process that depends both on the strain history (i.e., the size of the ridges) and the local ability of the lithosphere to support a load. Few triple bands are observed at latitudes higher than +/− 60°, for example, perhaps because of the greater thickness of the ice shell toward the poles. Subsequent brightening and ultimate erasure takes place over time scales which may depend on the rate of topographic relaxation (faster near the equator) or the flux of charged particles (greater on the trailing side).

While we cannot be sure that any given crack will evolve into a ridge, or ridge into a triple band, we can assert with some confidence that the bright ancient bands seen in the multispectral data are the products of formerly dark red–brown lineae such as triple bands, and that the presently prominent triple bands started out as mere incipient cracks. This is sufficient for the purpose of interpreting the results of the next section.

TABLE II
Evolution of Lineaments

Lineament type	Morphology	Color/albedo	Age
Fractures	narrow (<1 km); negative relief	Generally colorless; may expose colored subsurface materials	youngest
Ridges	raised relief (100–200 m) double or multiple ridge sets; 1–5 km wide.	initially bright blue, deep 1 μm absorption; possible frost cover during active phase	younger
Triple bands	multiple ridge sets flanked by smooth, dark margins	bright blue to dark red ridges; darker red–brown margins	older
Ancient bands	presumed similar to triple bands, perhaps relaxed.	intermediate in color between triple bands and icy plains; brighter than plains at long wavelengths	oldest

5. ORIENTATION OF LINEAMENTS

Because of the diverse spectral and morphological characteristics of europan lineaments, their orientations can be mapped without presupposing any particular model for their formation. Both the bright ancient bands and the dark triple bands can be easily distinguished on the basis of their color and albedo contrast with the icy plains. These spectral units were mapped in the area of G1 four-color coverage using a supervised classification approach. Spectra of "type areas" representative of the target lineaments were measured from images photometrically corrected for illumination and viewing geometry using a Lunar–Lambert function of the form (Buratti 1984, McEwen 1991)

$$R_F = R_0[2L\mu_0/(\mu_0 + \mu) + (1 - L)\mu_0],$$

where R_F is the recorded radiance, R_0 is the corrected radiance or normal albedo, μ_0 and μ are the cosines of the incidence and emission angles, respectively, and L is an empirically chosen constant equal to 0.4 (here assumed independent of wavelength). This value of L best serves to flatten the brightness variations across the disk of Europa, particularly at longer wavelengths. Qualitatively similar distributions result from the spectral mapping when a value of $L = 0.7$ (Buratti and Veverka 1983) is used instead.

Each pixel in the image cube is compared to the reference spectra of the type areas and accepted as a member of the class if it falls within a given range of the target mean radiance at every wavelength, where the range is specified in terms of the target spectrum's standard deviation. Each type area is classified independently, and the results are combined to form classes. Type areas defined for the triple bands included Minos, Cadmus, and Asterius Lineae. Areas chosen to be representative of the ancient bands include the bright wedge AB5 and several lineae running parallel to the wedge that could clearly be seen to predate the triple bands. Both types of lineae were sampled at several points along their lengths, to allow for imperfections in the photometric correction. The younger incipient cracks in this area cannot be mapped on the basis of their color characteristics and were simply defined to include all narrow fractures younger than the triple bands without discernible relief or color differences; they were traced along their lengths in the green filter image—the sharpest of the four-color set.

The results are shown in Fig. 13. The stratigraphically oldest lineaments, those with spectral reflectance similar to the bright wedge AB5, generally tend to have southwest–northeast orientations (Fig. 13A). The intermediate aged triple bands trend generally east–west (Fig. 13B), while the youngest lineaments have northwest–southeast trends, roughly radial to the antijove point (Fig. 13C). In this part of Europa, the orientations of the lineaments vary systematically with age, suggesting that the principal stress directions have rotated clockwise over time. Several as-

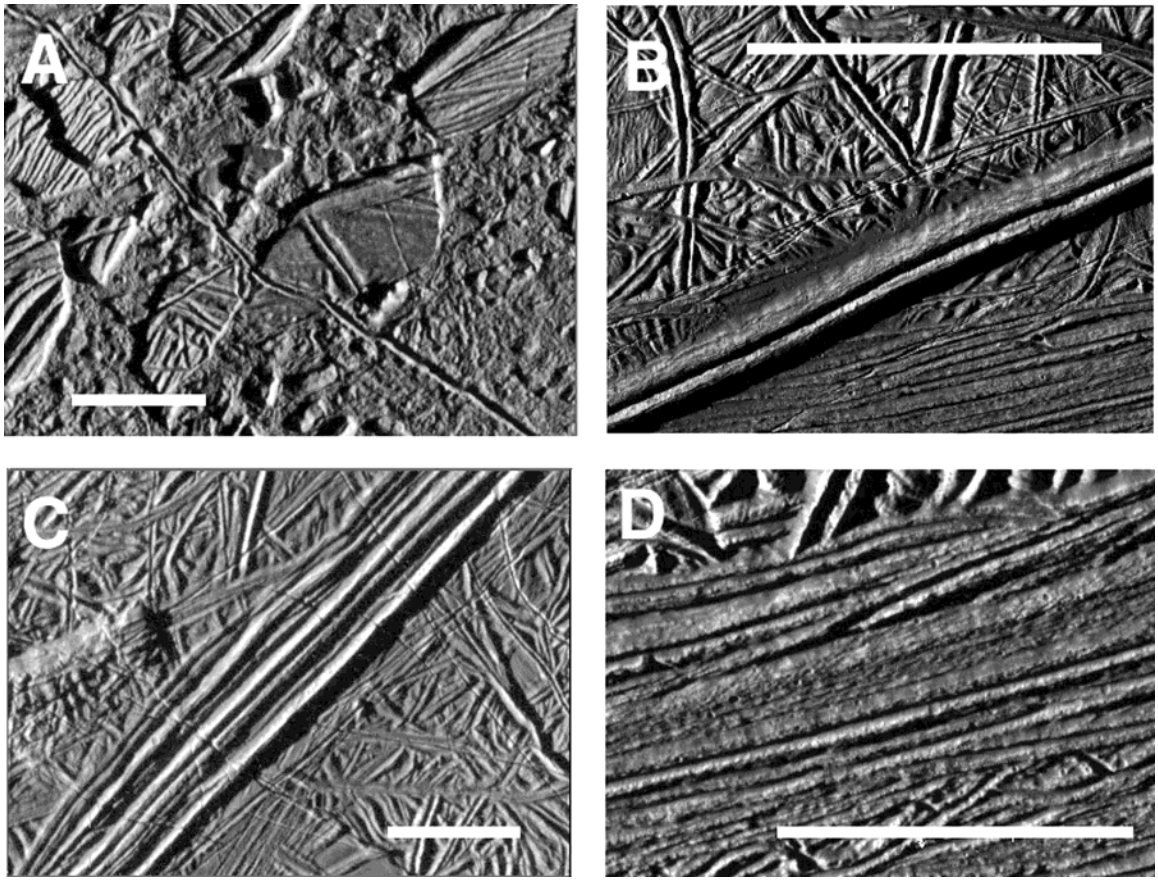

FIG. 12. High-resolution examples of lineaments representative of (A) simple fractures, (B) double-ridges, (C) multiple ridged triple bands (Asterius Linea) and (D) ancient, topographically relaxed bands. Scale bars are 5 km (picture numbers E6E0051 (A), E6E0050 (C), E6E0074 (B and D)).

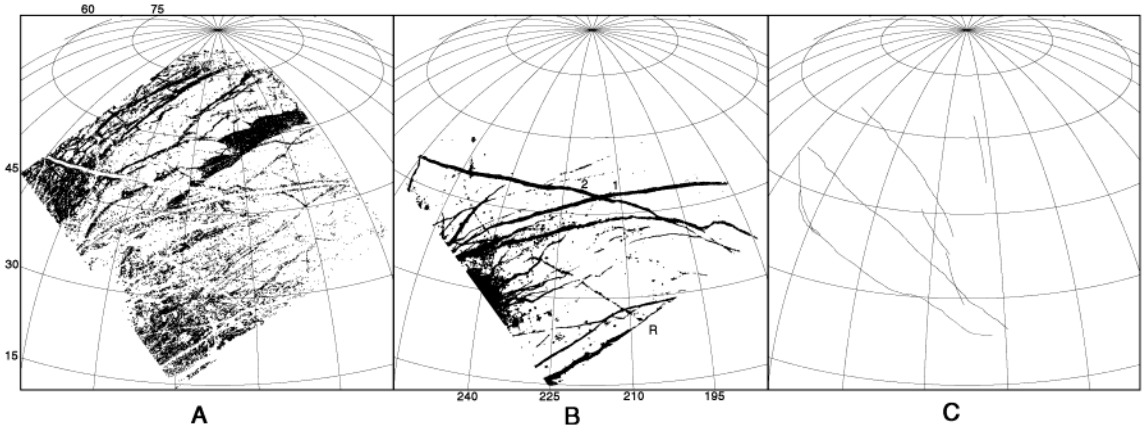

FIG. 13. Spectral maps showing systematic rotation of lineaments with stratigraphic age. (A) Bright ancient bands trend southwest–northeast; (B) dark, intermediate aged triple bands trend generally east–west; young incipient fractures trend northwest–southeast, roughly radial to the antijove point. In (B), ''1'' and ''2'' refer to the order of placement of two prominent triple bands, Minos (TB3) and Cadmus (TB1) Lineae, while ''R'' marks Rhadamanthys Linea (Fig. 10).

pects of the spectral mapping results should be emphasized. First, the maps show the average orientations of numerous bands interpreted to be widely separated in age. The general sense of rotation is suggested by the crosscutting relationships at several major lineament intersections—for example, the younger of the two prominent triple bands (Cadmus Linea, marked ''2'' in Fig. 13B) has a more northwesterly trend than the older (Minos Linea, marked ''1''), consistent with clockwise rotation. However, there are numerous exceptions to this rule, particularly among lineae of similar age, and intersections between particular pairs of bands often run counter to the general trend. Reasons for this may include the tendency for faults to follow preexisting crustal weaknesses and the occurrence of fractures in conjugate sets. We are aided in our analysis by the facts that relationships are established over a wide area (the images extend over 1500 km in the east–west direction), between lineaments distinctly different in age, and between lineaments that have certain morphological elements in common, including great lengths and straight, nearly linear planforms—no wedges and few arcuate ridges are present in the region. An interesting detail is the inclusion of the margins of Minos with the older bright materials, in agreement with other indications that bands begin brightening along their outside edges (Section 3). Finally, we note that Rhadamanthys Linea (marked ''R'' in Fig. 13B) has spectral characteristics similar to fully developed triple bands, but an orientation closer to that of the youngest fractures (Fig. 13C). As mentioned in Section 3, Rhadamanthys' morphology is also transitional between that of fractures/ridges and that of triple bands, supporting the suggestion (Belton *et al.* 1996) that the lineament may be a triple band seen at an early stage of formation.

Nonsynchronous planetary rotation may provide an explanation for the apparent changes in orientation of the northern hemisphere lineaments (Geissler *et al.* 1998). Calculations by Greenberg and Weidenschilling (1984) predict that Europa may rotate slightly faster than the synchronous rate, due to tidal torques caused by Europa's orbital eccentricity. As Europa's surface is reoriented relative to the tidal figure, the pattern of stresses experienced in the northern hemisphere should rotate clockwise, consistent with the observations (Fig. 14). This is equally true whether the fractures are produced by the daily tidal distortions (Helfenstein and Parmentier 1980) or by the long-term stresses induced by nonsynchronous rotation itself (Helfenstein and Parmentier 1985, McEwen 1986a). Interestingly, the orientation of the youngest fractures (incipient cracks, along with Rhadamanthys Linea) is roughly radial to the antijove point. This is not consistent with the stress pattern predicted for nonsynchronous rotation, which is displaced 45° to the east (Helfenstein and Parmentier 1985), but instead fits the current tidal stress regime. The lineaments may be produced by diurnal stresses due to

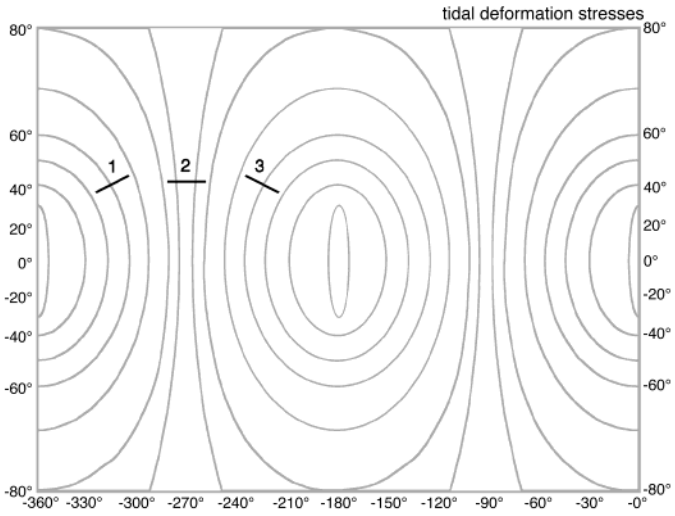

FIG. 14. Clockwise rotation of stress directions over time as a result of nonsynchronous planetary rotation. As the surface gradually migrates eastward, it fractures in the direction perpendicular to the maximum tensile stresses (shown as contours).

Europa's forced eccentricity, but shifted eastward by nonsynchronous rotation over much longer time scales (cf. Greenberg *et al.* 1998).

6. AN ACTIVE LINEAMENT?

Of Europa's many diverse lineaments, Agenor Linea demands particular attention. Only partially imaged by Voyager, Agenor and its short companion Katreus Linea to the north were seen as narrow E–W trending bands that were brighter than comparable lineaments and younger than any others in the region (Pieri 1981, Lucchitta *et al.* 1981, Lucchitta and Soderblom 1982, Schenk and McKinnon 1989). Galileo has now mapped the entire 1500-km length of Agenor at moderate resolution (Fig. 15) and measured the spectral and photometric properties of this interesting feature. It is located in southern mid latitudes from 37° to 44° S, and closely circumscribes the equatorial rift zone of wedge-shaped bands west of the antijove point. Its position and orientation are such that its maximum diurnal tensional stress (due to tidal flexing, as Europa orbits Jupiter) coincides with the tensional stress due to long-term rotational reorientation (Greenberg *et al.* 1998, Hoppa *et al.* 1998), making it a likely candidate for recent and perhaps current activity. Agenor was noted in high phase angle Voyager images to be relatively blue at visible wavelengths compared to other europan terrains (Schenk and McKinnon 1989). From Galileo data it is now clear that Agenor's color is markedly phase-angle dependent. Measured at low phase (2.2°, during G2) its spectrum is relatively neutral, similar to the bright rays of crater Pwyll.

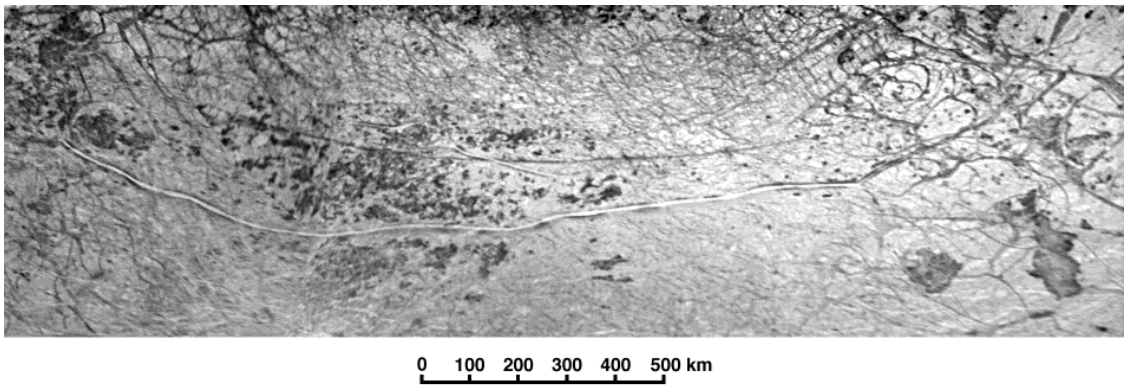

FIG. 15. Agenor Linea, shown in a mosaic of clear-filter images from Galileo's 4th and 6th orbits (picture numbers E4E0002, E6E0001, and E6E0002).

The lineament has a higher 968/green ratio (~1.0) than the adjacent plains (~0.93) and a slightly lower violet/green ratio. However, at higher phase (100.5°, E12) this trend is reversed. Agenor is much ''bluer'' than the surrounding plains, with a 968/green ratio of ~0.83 (among the lowest values measured on Europa) and a higher violet/green ratio than the nearby plains. Agenor's high albedo, high violet/green ratio, and deep 1-μm absorption at high phase angles suggest a surface made up of clean, relatively coarse-grained ice. A diffuse, high-albedo halo surrounding the western reaches of Agenor is hinted in the G2 global color images.

Agenor also appears to have an unusual photometric function in comparison to the neighboring plains (Fig. 16). It is darker than its surroundings at low phase angles (2.2°, at 6.9 km/pixel during G2), comparable at intermediate phase angles (36.9°, at 1.6 km/pixel in E6), but much brighter at high phase angles (56° in E4 at 1.2 km/pixel, and 93.7° in the 1.8 km/pixel Voyager 2 observation). Its relative reflectance, normalized to that of the surrounding surfaces, can be approximated as a linear function of phase angle with a coefficient (phase constant) of 4.4×10^{-3}/degree. Agenor's photometric behavior suggests a surface cover of relatively forward-scattering particles in comparison to more typical europan icy materials, such as a thin mantle of frost. If so, the deposits may indicate recent (or current) activity along the lineament, since sputtering erosion and deposition processes are expected to homogenize the photometric properties of Europa over short time periods (Cheng *et al.* 1986).

7. DISCUSSION

Galileo data have provided a number of new observational constraints on the morphology and spectral properties of europan lineaments which must be satisfied by any model that successfully explains their formation and evolution. High-resolution images reveal ridges at the cores of the lineaments, which occur in pairs or bilaterally symmetric sets with central valleys. These ridges seem to have a characteristic maximum size (Kadel *et al.* 1998) and are generally uniform in height and width along their lengths, which sometimes extend to great distances. Older ridges have subdued relief in comparison to their younger counterparts. Marginal fractures running parallel to some ridges suggest flexure of the surface under their weight. Color observations suggest that the ridges are extruded as relatively clean ice, whereas the spectra of dark lineae indicate contamination with a nonice component. Triple bands apparently form when the ice surfaces adjacent to a ridge darken and redden while the ridge itself remains bright in comparison to the band margins. The lineaments brighten after activity along them ceases, exceeding the albedo of the undisturbed icy plains at longer wavelengths.

The mechanisms of lineament formation and evolution are not known, although a variety of hypotheses have been suggested. One scenario for producing ridges supposes that fracturing of the surface allows less dense material to rise from below. The buoyant material could be warm, convective ice (Head *et al.* 1997) or gas-charged liquids which produce cryoclastic eruptions upon reaching the surface (Greeley *et al.* 1998). Such density instabilities are unlikely to have topographic expressions which are uniform along the lengths of the fractures, however, and neither model easily explains the central valleys characteristic of europan ridges. Alternatively, the ridges may result from repeated motion of rigid crustal plates floating on a subsurface ocean, for example by ductile deformation of the solid plate margins or by ''pumping'' of material from the interior (Greenberg *et al.* 1998).

Also mysterious are the means by which ice near ridges darkens and reddens, and the mechanism and time scale for brightening of the bands. Much of the uncertainty concerns the nature of the nonice component that colors the

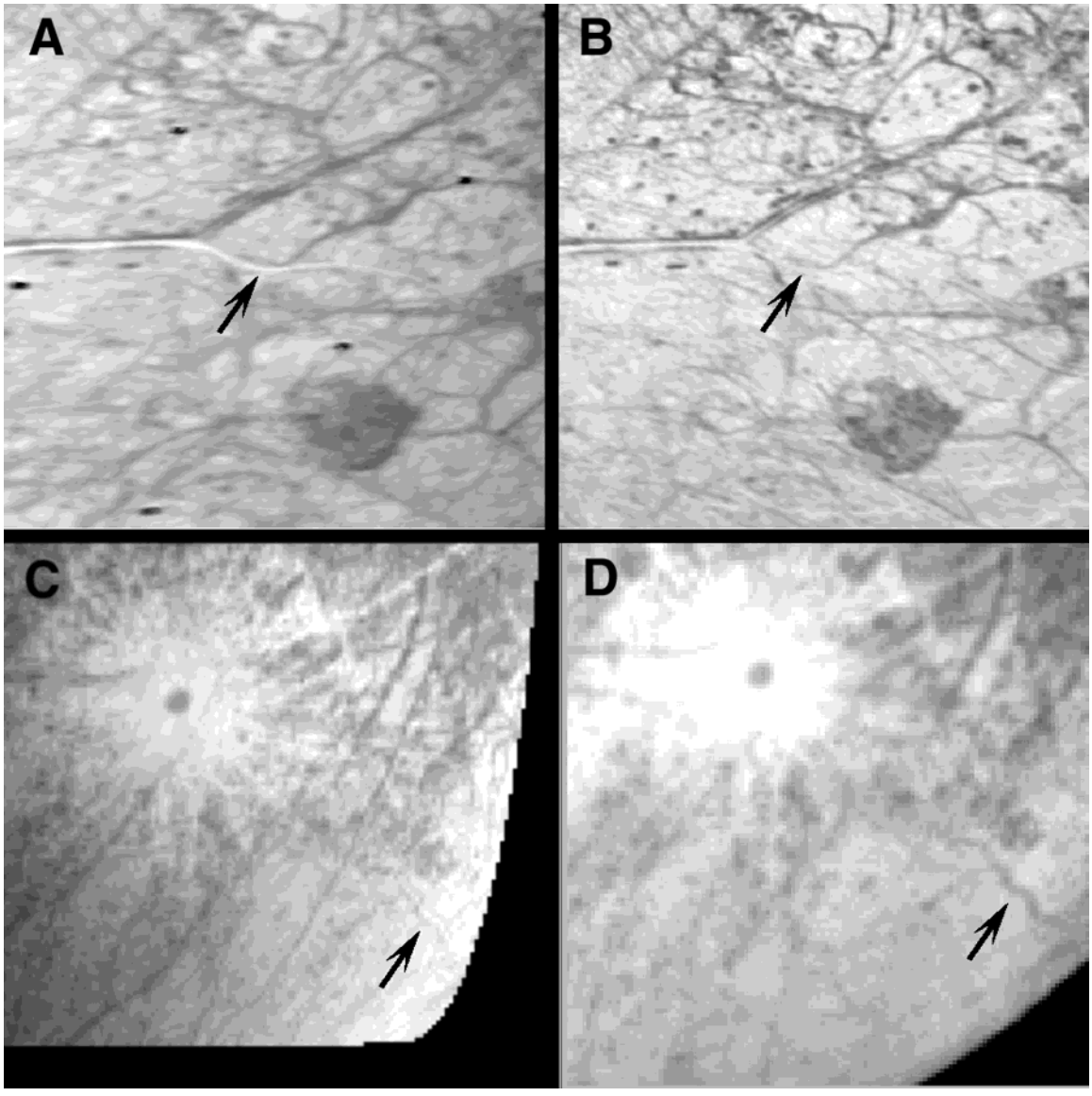

FIG. 16. Comparison of Agenor Linea's appearance at various phase angles. (A) Voyager 2, clear filter, 93.7°, (B) E4, clear filter, 56°, (C) E6, clear filter, 36.9°, (D) G2, green filter, 2.2° (picture numbers 1255J2–001 (A), E6E0001 (B), E4E0002 (C), G2E0001 (D)).

triple bands, craters, and disrupted terrain everywhere on the satellite. As pointed out previously, the sulfate hydrates regarded most likely to account for the ultraviolet and infrared spectral reflectance of the dark materials are colorless at visible wavelengths. Another component is needed to explain the visible coloration. One possibility is that the sulfates break down under irradiation by charged particles to form colored sulfur compounds. Ordinary orthorhombic sulfur (S_8) provides a poor match to the visible and near-infrared continuum observed by SSI, however. Attempts to model the dark materials' six-wavelength SSI spectrum as a mixture of sulfur and ice, using the surface scattering models of Hapke (1981, 1986) with parameters derived by Domingue *et al.* (1991), result in serious mismatches to the observations and minimum χ^2 values in the hundreds. Other inorganic compounds such as monatomic sulfur or sodium sulfides have yet to be examined as potential compositional candidates. On the other hand, a much better fit ($\chi^2 = 2$) is obtained from a mixture made up of 2% organic ice tholins (Khare *et al.* 1993) with 100-μm sized water ice grains. The presence of organics is suggested by weak absorptions in NIMS spectra at 3.47 and 4.5 μm, interpreted to be due to C–H and C–N, respectively (Smythe *et al.* 1998). Organic compounds are also interpreted from NIMS data on Callisto and Ganymede (McCord *et al.* 1997). Interestingly, aqueous organic complexes

should be expected to brighten upon exposure to the surface of Europa. McDonald and Ockert-Bell (1997) present the results of a laboratory experiment in which an organic sample with water frost was irradiated by low-energy charged particles. The sample's visible absorbance was measurably reduced as the carbon–carbon double bonds transformed into single bonds by reactions with water radiolysis products: simple organic breakdown that ultimately leads to carbon dioxide. Because they are soluble, the tholins (or similar compounds) could be dissolved along with salts and other materials in a subsurface liquid layer and exposed wherever the surface has been penetrated by impactors, melted from below, or fractured by changing global stresses.

8. SUMMARY

Galileo imaging observations have enlarged our knowledge of europan lineaments in two fundamental ways. First, high-resolution images have sampled these landforms in several different locations, shedding light on the morphological characteristics of lineae in various stages of development. Second, multispectral observations in the near-infrared have revealed ancient lineae scarcely distinguishable at shorter wavelengths, allowing inference of systematic changes in the orientation of the lineaments with time. The new insights provided by Galileo and their possible implications may be summarized as follows:

1. Indications from both the high-resolution and color data suggest that the lineaments progress through an evolutionary sequence over time. All start out as simple cracks, but favorably positioned fractures form marginal ridges, a process which may be repeated until multiple ridged triple bands develop. These bands ultimately brighten and viscously relax, leaving a landscape crisscrossed with a network of chaotically interwoven lineae.

2. The youngest lineaments seem to be tensional fractures which meander and change direction, taking advantage of preexisting crustal weaknesses. The youngest fractures visible in the G1 color observations are oriented roughly radial to the antijove point, suggesting that these particular lineaments formed in response to tidal stresses.

3. Lineament formation appears to be the dominant resurfacing mechanism on Europa, and every landscape that has escaped erasure by heating from below is imprinted with generation after generation of intersecting ridges at various scales and orientations. Recently developed ridges appear to be made up of relatively clean ice, suggesting segregation of materials from the murky interior. The colors of the cracks and ridges may account for the distinctive hue of the satellite in comparison to the other icy moons of Jupiter.

4. Based on the few triple-bands so far imaged at high resolution, the dark, red–brown coloration of ice surfaces adjacent to ridges and multiple-ridge sets becomes evident only after activity along the lineament ceases. The color of triple bands is indistinguishable from that of thermally disrupted terrain and ejecta of recent craters like Pwyll, suggesting a single, as yet unidentified nonice contaminant which is uniformly distributed in the shallow subsurface.

5. Ancient bands are observed to have brightened at long wavelengths beyond the albedo of the undisturbed icy plains and not merely faded as believed on the basis of Voyager data. Because bands brighten and ultimately disappear, the continued presence of dark lineaments may place constraints on the age of geologic activity on Europa.

6. Spectral mapping of lineaments in Europa's north polar region suggests a clockwise rotation of stress direction with time, consistent with faster-than-synchronous planetary rotation.

7. Agenor Linea's spectral and photometric properties are consistent with a surface covering of frost, suggesting recent or perhaps current activity along this unusual lineament. Agenor is targeted for high-resolution, stereo, and color observations during Galileo's extended mission, beginning with orbit E16 in July, 1998.

ACKNOWLEDGMENTS

We thank B. K. Lucchitta and B. J. Buratti for constructive reviews and J. M. Moore for helpful discussion. The spectral modeling was performed at Cornell University under the direction of the late Carl Sagan and with the help of P. Wilson, G. McDonald and W. Calvin.

REFERENCES

Belton, M. J. S., K. P. Klaasen, M. C. Clary, J. L. Anderson, C. D. Anger, M. H. Carr, C. R. Chapman, M. E. Davies, R. Greeley, D. Anderson, L. K. Bolef, T. E. Townsend, R. Greenberg, J. W. Head III, G. Neukum, C. B. Pilcher, J. Veverka, P. J. Gierasch, F. P. Fanale, A. P. Ingersoll, H. Masursky, D. Morrison, and J. B. Pollack 1992. The Galileo solid-state imaging experiment. *Space Sci. Rev.* **60,** 413–455.

Belton, M. J. S., J. Head, A. Ingersoll, R. Greeley, A. McEwen, K. Klaasen, D. Senske, R. Pappalardo, G. Collins, A. Vasavada, R. Sullivan, D. Simonelli, P. Geissler, M. Carr, M. Davies, J. Veverka, P. Gierasch, D. Banfield, M. Bell, C. Chapman, C. Anger, R. Greenberg, G. Neukum, C. Pilcher, R. Beebe, J. Burns, F. Fanale, W. Ip, T. V. Johnson, D. Morrison, J. Moore, G. Orton, P. Thomas, and R. West 1996. Galileo's first images of Jupiter and the Galilean satellites. *Science* **274,** 377–385.

Buratti, B. 1984. Voyager disk-resolved photometry of the saturnian satellites. *Icarus* **59,** 392–405.

Buratti, B., and J. Veverka 1983. Voyager photometry of Europa. *Icarus* **55,** 93–110.

Carlson, R., W. Smythe, K. Baines, E. Barbinis, K. Becker, R. Burns, S. Calcutt, W. Calvin, R. Clark, G. Danielson, A. Davies, P. Drossart, T. Encrenaz, F. Fanale, J. Granahan, G. Hansen, P. Herrera, C. Hibbitts, J. Hui, P. Irwin, T. Johnson, L. Kamp, H. Kieffer, F. Leader, E. Lellouch, R. Lopes-Gautier, D. Matson, T. McCord, R. Mehlman, A. Ocampo, G. Orton, M. Roos-Serote, M. Segura, J. Shirley, L. Soderblom, A.

Stevenson, F. Taylor, J. Torson, A. Weir, and P. Weissman 1996. Near-infrared spectroscopy and spectral mapping of Jupiter and the Galilean satellites: Results from Galileo's initial orbit. *Science* **274,** 385–388.

Cheng, A. F., P. K. Haff, R. E. Johnson, and L. J. Lanzerotti 1986. Interactions of planetary magnetospheres with icy satellite surfaces. In *Satellites of Jupiter* (D. Morrison, Ed.), pp. 403–436. Univ. of Arizona Press, Tucson.

Clark, B. E., P. Helfenstein, J. Veverka, M. Ockert-Bell, R. J. Sullivan, P. E. Geissler, C. B. Phillips, A. S. McEwen, R. Greeley, G. Neukum, T. Denk, K. Klaasen, and the Galileo SSI Team 1998. Multispectral terrain analysis of Europa from Galileo images. *Icarus* **135,** 95–106.

Domingue, D. L., B. W. Hapke, G. W. Lockwood, and D. T. Thompson 1991. Europa's phase curve—Implications for surface structure. *Icarus* **90,** 30–42.

Fanale, F., J. Granahan, T. McCord, G. Hansen, R. Carlson, D. Matson, A. Ocampo, L. Kamp, W. Smythe, F. Leader, R. Mehlman, R. Greeley, R. Sullivan, P. Geissler, C. Barth, A. Hendrix, B. Clark, P. Helfenstein, J. Veverka, M. J. S. Belton, K. Becker, and T. Becker 1998, Galileo's multi-instrument spectral view of Europa's surface composition. *Icarus,* submitted.

Geissler, P., W. R. Thompson, R. Greenberg, J. Moersch, A. McEwen, and C. Sagan 1995. Galileo multispectral imaging of Earth. *J. Geophys. Res.* **100,** 16,895–16,906.

Geissler, P., R. Greenberg, G. Hoppa, P. Helfenstein, A. McEwen, R. Pappalardo, R. Tufts, M. Ockert-Bell, R. Sullivan, R. Greeley, M. J. S. Belton, T. Denk, B. Clark, J. Burns, J. Veverka, and the Galileo Imaging Team 1998. Evidence for non-synchronous rotation of Europa. *Nature* **391,** 368–371.

Geissler, P., C. Phillips, and T. Denk 1996. The color of Europa: Comparisons with Ganymede, Callisto and Antarctica (No. 8.5). *Workshop on Remote Sensing of Planetary Ices: Earth and other Solid Bodies*, Flagstaff, Arizona, June 11–13, 1996. [Abstract]

Greeley, R., R. Sullivan, J. Klemaszewski, K. Homan, J. W. Head III, R. T. Pappalardo, J. Veverka, B. E. Clark, T. Johnson, K. P. Klaasen, M. Belton, J. Moore, E. Asphaug, M. H. Carr, G. Neukum, T. Denk, C. R. Chapman, C. B. Pilcher, P. E. Geissler, R. Greenberg, and R. Tufts 1998. Europa: Initial Galileo geological observations. *Icarus* **135,** 4–24.

Greenberg, R., and S. Weidenschilling 1984. How fast do Galilean satellites spin? *Icarus* **58,** 186–196.

Greenberg, R., P. Geissler, G. Hoppa, B. R. Tufts, D. D. Durda, R. Pappalardo, J. W. Head, R. Greeley, R. Sullivan, and M. H. Carr 1998. Tectonic processes on Europa: Tidal stresses, mechanical response, and visible features. *Icarus* **135,** 64–78.

Hapke, B. 1981. Bidirectional reflectance spectroscopy. 1. Theory. *J. Geophys. Res.* **86,** 4571–4586.

Hapke, B. 1986. Bidirectional reflectance spectroscopy. IV—The extinction coefficient and the opposition effect. *Icarus* **67,** 264–280.

Head, J. W., R. T. Pappalardo, R. Greeley, R. J. Sullivan, C. Pilcher, G. Schubert, W. Moore, M. Carr, J. Moore, and M. Belton 1997. Evidence for recent solid-state convection on Europa: The nature of pits, domes, spots, and ridges. *Bull. Am. Astron. Soc.* **29,** 983. [Abstract]

Helfenstein, P., and A. F. Cook 1984. Active venting of Europa? Analysis of a transient bright surface feature. *Lunar Planet. Sci. Conf.* **XV,** 354–355. [Abstract]

Helfenstein, P., and E. M. Parmentier 1980. Fractures on Europa: Possible response of an ice crust to tidal deformation. *Proc. Lunar Planet. Sci. Conf. 11th*, pp. 1987–1998.

Helfenstein, P., and E. M. Parmentier 1983. Patterns of fracture and tidal stresses on Europa. *Icarus* **53,** 415–430.

Helfenstein, P., and E. M. Parmentier 1985. Patterns of fracture and tidal stresses due to nonsynchronous rotation: Implications for fracturing on Europa. *Icarus* **61,** 175–184.

Helfenstein, P., N. Currier, B. E. Clark, J. Veverka, M. Bell, R. Sullivan, J. Klemaszewski, R. Greeley, R. T. Pappalardo, J. W. Head III, T. Jones, K. Klaasen, K. Magee, P. Geissler, R. Greenberg, A. McEwen, C. Phillips, T. Colvin, M. Davies, T. Denk, G. Neukum, and M. J. S. Belton 1998. Galileo observations of Europa's Opposition Effect. *Icarus* **135,** 41–63.

Hendrix, A. R., C. A. Barth, C. W. Hord, A. I. Stewart, W. R. Pryor, K. E. Simmons, W. E. Mcclintock, J. J. Gebben, J. M. Ajello, K. L. Naviaux, J. J. Aiello, A. L. Lane, W. K. Tobiska, and S. K. Stephens 1996. Galileo ultraviolet spectrometer observations of Europa. *Bull. Am. Astron. Soc.* **28,** 1140.

Hoppa, G., R. Greenberg, P. Geissler, B. R. Tufts, C. B. Phillips, D. Durda, and the Galileo Imaging Team 1998. Comparison of global stress models with geographical features on Europa. *Lunar Planet. Sci. XXIX*, Abstract 1865, Lunar and Planetary Institute, Houston. [CD-ROM]

Johnson, T. V., J. A. Mosher, P. Kupferman, L. A. Soderblom, G. E. Danielson, and A. F. Cook 1983. Global multispectral mosaics of the icy Galilean satellites. *J. Geophys. Res.* **88,** 5789–5805.

Kadel, S. D., S. A. Fagents, and R. Greeley 1998. Trough-bounding ridge pairs on Europa—Considerations for an endogenic model of formation. *Lunar Planet. Sci. XXIX*, Abstract 1078. Lunar and Planetary Institute, Houston. [CD-ROM]

Klaasen, K., M. Belton, H. Breneman, A. McEwen, M. Davies, R. Sullivan, C. Chapman, G. Neukum, C. Heffernan, A. Harch, J. Kaufman, W. Merline, L. Gaddis, W. Cunningham, P. Helfenstein, and T. Colvin 1997. Inflight performance characteristics, calibration, and utilization of the Galileo SSI camera. *Opt. Eng.* **36,** 3001–3027.

Leith, A. C., and W. B. McKinnon 1996. Is there evidence for polar wander on Europa? *Icarus* **120,** 387–398.

Lucchitta, B. K., L. A. Soderblom, and H. M. Ferguson 1981. Structures on Europa. *Proc. Lunar Planet. Sci.* **12,** 1555–1567.

Lucchitta, B. K., and L. A. Soderblom 1982. Geology of Europa. In *Satellites of Jupiter* (D. Morrison, Ed.), pp. 521–555. Univ. of Arizona Press, Tucson.

McCord, T. B., R. Carlson, W. Smythe, G. Hansen, R. Clark, C. Hibbitts, F. Fanale, J. Granahan, M. Segura, D. Matson, T. Johnson, and P. Martin 1997. Organics and other molecules in the surfaces of Callisto and Ganymede. *Science* **278,** 271–275.

McCord, T. B., G. Hansen, F. P. Fanale, R. W. Carlson, D. Matson, T. V. Johnson, W. Smythe, J. K. Crowley, P. D. Martin, A. Ocampo, C. A. Hibbitts, J. C. Granahan, and the Galileo NIMS team 1998. Salts on Europa's Surface From the Galileo NIMS Investigation. *Lunar Planet. Sci. XXIX*, Abstract 1560. Lunar and Planetary Institute, Houston. [CD-ROM]

McDonald, G. D., and M. E. Ockert-Bell 1997. Oxidative destruction of polymeric material on the surface of Europa. *Lunar Planet. Sci. XXIII*, Abstract 1475. Lunar and Planetary Institute, Houston. [CD-ROM]

McEwen, A. S. 1986a. Tidal reorientation and the fracturing of Jupiter's moon Europa. *Nature* **321,** 49–51.

McEwen, A. S. 1986b. Exogenic and endogenic albedo and color patterns on Europa. *J. Geophys. Res.* **91,** 8077–8097.

McEwen, A. S. 1991. Photometric functions for photoclinometry and other applications. *Icarus* **92,** 298–311.

Moore, J. M., E. Asphaug, R. J. Sullivan, J. E. Klemaszewski, K. C. Bender, R. Greeley, P. E. Geissler, A. S. McEwen, E. P. Turtle, C. B. Phillips, B. R. Tufts, J. W. Head III, R. T. Pappalardo, K. B. Jones, C. R. Chapman, M. J. S. Belton, R. L. Kirk, and D. Morrison 1998. Large impact features on Europa: Results of the Galileo nominal mission. *Icarus* **135,** 127–145.

Ojakangas, G. W., and D. J. Stevenson 1989a. Thermal state of an ice shell on Europa. *Icarus* **81,** 220–241.

Ojakangas, G. W., and D. J. Stevenson 1989b. Polar wander of an ice shell on Europa. *Icarus* **81,** 242–270.

Pappalardo, R. T., and M. Coon 1996. A sea-ice analog for the surface of Europa. *Lunar Planet. Sci. Conf. XXVII*, pp. 997–998.

Pappalardo, R. T., and R. J. Sullivan 1996. Evidence for crustal separation on Europa. *Icarus* **123,** 557–567.

Pieri, D. C. 1981. Lineament and polygon patterns on Europa. *Nature* **289,** 17–21.

Schenk, P. M., and W. B. McKinnon 1989. Fault offsets and lateral crustal movement on Europa: Evidence for a mobile ice shell. *Icarus* **79,** 75–100.

Smith, B. A., L. A. Soderblom, T. V. Johnson, A. Ingersoll, S. A. Collins,. E. M. Shoemaker, G. E. Hunt, H. Masursky, M. Carr, M. E. Davies, A. F. Cook, J. Boyce, G. E. Danielson, T. Owen, C. Sagan, R. Beebe, J. Veverka, R. Strom, J. McCauley, D. Morrison, G. Briggs, and V. E. Soumi 1979a. The Jupiter system through the eyes of Voyager 1. *Science* **204,** 951–972.

Smith, B. A., L. A. Soderblom, R. Beebe, J. Boyce, G. Briggs, M. Carr, S. A. Collins, A. F. Cook, G. E. Danielson, M. E. Davies, G. E. Hunt, A. Ingersoll, T. V. Johnson, H. Masursky, J. McCauley, D. Morrison, T. Owen, C. Sagan, E. M. Shoemaker, R. Strom, V. E. Soumi, and J. Veverka 1979b. The Galilean satellites and Jupiter: Voyager 2 imaging results. *Science* **206,** 927–950.

Smythe, W. D., R. W. Carlson, A. Ocampo, D. Matson, T. V. Johnson, T. B. McCord, G. E. Hansen, L. A. Soderblom, and R. N. Clark 1998. Absorption bands in the spectrum of Europa detected by the Galileo NIMS instrument. *Lunar Planet. Sci. Conf. XXIX*, Abstract 1532. Lunar and Planetary Institute, Houston. [CD-ROM]